Calibrated Measurement of Optoelectronic Frequency Response

Paul D. Hale, *Senior Member, IEEE,* and Dylan F. Williams, *Fellow, IEEE*

***Abstract*—We describe the most straightforward method for accurately measuring the frequency response of optoelectronic devices. The method uses a calibrated optical reference receiver, a modulated optical source, and a calibrated electrical vector network analyzer.**

***Index Terms*—Calibration, frequency response, measurement, optoelectronic devices, scattering matrices.**

I. Introduction

WE DESCRIBE how a calibrated electrical vector network analyzer (VNA), modulated optical source, and calibrated optical reference receiver are used to accurately measure the frequency response of a large class of optoelectronic devices including Mach–Zehnder modulators, electroabsorption modulators, directly modulated semiconductor lasers, and linear optical receivers. Although this type of measurement system is commonly used in the optoelectronics community, the theory behind the measurements and the procedures and restrictions necessary for accurate calibration are not generally well known. Indeed, there are several competing approaches to optical and optoelectronic network analysis in the literature, some of which may not be justified given the physics of the optoelectronic interactions and the limited information that the simple measurement system can provide.

To clarify the operation of these systems and their limitations, we develop a simple optoelectronic scattering matrix formalism that is consistent with standard microwave theory and practice. The formalism relates the optical modulation envelope at one port of the device to the electrical wave at the other port and describes the performance of optical receivers and modulated optical sources. We then apply the formalism to calibration of the optoelectronic measurement system and demonstrate with some simple examples.

Our formalism requires that no optical signals propagate in the reverse direction between the modulated optical source and receiver to eliminate interference of the optical carrier with itself that cannot be accounted for by the test equipment or the scattering matrix formalism. To the best of our knowledge, this restriction has never been discussed in the literature. In Section IX, we discuss the reasons for this restriction and compare our treatment with other optoelectronic scattering matrix formalisms and measurement methods in the literature.

Manuscript received January 29, 2002.

The authors are with the National Institute of Standards and Technology, Boulder, CO 80305 USA (e-mail: hale@boulder.nist.gov).

Digital Object Identifier 10.1109/TMTT.2003.809186

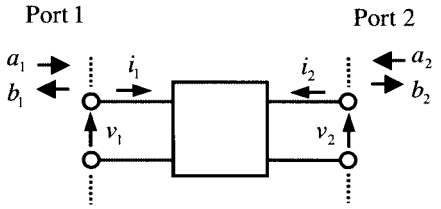

Fig. 1. Schematic showing waves flowing in and out of component. Ports 1 and 2 are represented by dotted lines.

The calibration and measurement procedure we describe in this paper is easier to perform than the one we previously described in [1]: the calibrated VNA performs all of the electrical mismatch corrections automatically and it does not require a calibrated power meter. Lightwave component analyzers (LCAs) such as those described in [2] can also perform the measurements described here, and must also be calibrated. In Appendix V, we describe how to apply the method to calibration or verification of LCAs. Some of the theory and procedures we describe in this paper have been outlined in [3] and [4], and are similar to those recommended by LCA manufacturers [2].

Finally, Appendixes I–III discuss relations between the quantities measured by the VNA system described here and Thévenin and Norton equivalent sources, normalized receiver response, and the input drive voltage, input drive current, and π-voltages of modulated sources.

II. Electrical Scattering Matrices

We start by briefly reviewing standard microwave circuit theory [5], [6]. We explicitly define the electrical quantities we will use since their definitions effect our measured optoelectronic quantities.

Standard microwave circuit theory defines all electrical parameters in single-mode electrical waveguides connecting all devices. As illustrated in Fig. 1, we begin by defining a single-frequency sinusoidal voltage $\mathrm{Re}(ve^{j\omega t})$ and current $\mathrm{Re}(ie^{j\omega t})$ at each port, where $\mathrm{Re}(\cdot)$ gives the real part of its argument, v is the complex amplitude of the voltage, i is the complex amplitude of the current, ω is the frequency in radians per second, and t is the time. We also define an incident-wave amplitude a and a reflected-wave amplitude b at each port in terms of the voltage amplitude v and current amplitude i via

$$a = \frac{1}{2\sqrt{Z_r}}\left(v + iZ_r\right)$$
$$b = \frac{1}{2\sqrt{Z_r}}\left(v - iZ_r\right). \quad (1)$$

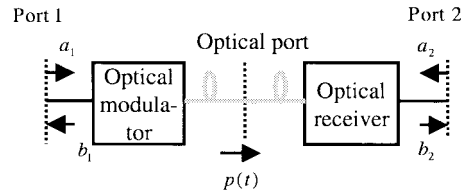

Fig. 2. Schematic showing electrical waves and optical power flowing in and out of an optoelectronic system. The electrical and optical ports are represented by dashed lines.

Here, Z_r is a real reference impedance, which is usually set to 50 Ω. These waves are the "pseudo-waves" of [6]. These waves correspond to the traveling waves in the waveguide [6] when the characteristic impedance of the waveguide is real and equal to Z_r.

The incident and reflected waves in (1) are scaled by the factor $\frac{1}{2}(Z_r)^{-1/2}$ so that the power P delivered to each port is

$$P = \frac{1}{2}\mathrm{Re}(vi*) = \frac{1}{2}\left(|a|^2 - |b|^2\right). \tag{2}$$

That is, the power crossing the reference plane at each port is the incident power $\frac{1}{2}|a|^2$ less the reflected power $\frac{1}{2}|b|^2$ leaving the port.

We call a one-port device with an impedance equal to Z_r a matched load. For a matched load $v = Z_r i$, the reflected wave amplitude $b = 0$ (i.e., the reflection coefficient $\Gamma \equiv b/a$ of a one-port matched load is zero), and the matched load completely absorbs the incident wave a.

Fig. 1 illustrates the incident and reflected waves at a two-port device, where subscripts "1" and "2" indicate the port number. The incident and reflected waves of a two-port device are related via the scattering or S-matrix $[S]$

$$\begin{bmatrix} b_1 \\ b_2 \end{bmatrix} = \begin{bmatrix} S_{11} & S_{12} \\ S_{21} & S_{22} \end{bmatrix} \begin{bmatrix} a_1 \\ a_2 \end{bmatrix}. \tag{3}$$

An electrical VNA calibrated in the conventional fashion measures the scattering parameters S_{ij} of the device with a reference impedance $Z_r = 50\ \Omega$ [6]. The elements of the S-matrix are dimensionless because they are ratios of the a and b waves. We call S_{11} a reflection coefficient and S_{21} the forward transmission coefficient of the device.

III. Scattering Matrices of Optoelectronic Systems

Let us determine the scattering parameters of the optoelectronic system shown in Fig. 2. It consists of two separate components connected by an optical fiber: an optical modulator (or directly modulated laser) on the left-hand side, and an optical receiver on the right-hand side. The system has a single electrical input port and a single electrical output port. The optical modulator uses electrical signals at its input port (port 1 in this figure) to linearly modulate the intensity (power) of the optical signal at the optical port. The receiver responds linearly to the optical power, not the carrier, and is sometimes called a square-law detector. Hence, the receiver linearly converts the intensity-modulated optical signal back into an electrical signal at its electrical output port (port 2 in this figure).

We require that the optical power $p(t)$ propagating in the forward direction at the optical port between the modulator and receiver, due to a single-frequency electrical excitation, be of the form [7]–[9]

$$p(t) = p_0 + p_0 m \cos(\omega t + \alpha). \tag{4}$$

In (4), m is a (real) modulation index and α is the phase of the modulation envelope. We do not restrict the frequency or phase modulation of the optical carrier because the optical receiver does not respond to the optical carrier: it only responds to the modulation envelope. The linear modulation described by (4) is generally available from directly modulated semiconductor lasers and integrated modulators that are suitably biased and driven by a small signal. We can reasonably neglect harmonics of the drive electrical signal generated by the modulator [10] because the VNA has a tuned receiver that effectively blocks the weak harmonics generated by real modulated sources.

As we stated earlier, we also require that there be no optical power propagating in the reverse direction (i.e., coming from or reflected by the receiver or other optical component). This constraint avoids optical interference that would further complicate (4). We discuss this further in Section IX.

The modulator reflects some of the electrical a_1 wave incident on the circuit from the left-hand side, generating an outgoing b_1 wave. However, since no optical power travels from right-hand side to the left across the optical port, a wave a_2 incident from the right-hand side cannot contribute to the outgoing b_1 wave. Thus, we have $b_1 = \Gamma_m\, a_1$, where Γ_m is the electrical reflection coefficient of the modulator.

We have already required that the modulator linearly modulate the power in the optical beam so the instantaneous optical power coming out of the modulator can be written as

$$p(t) = p_0 + \mathrm{Re}\left\{G a_1 e^{j\omega t}\right\} \tag{5}$$

where G is the complex response of the modulator. Since we have required that there be no optical interference at the optical port, we can equate the modulated signal generated by the modulator with the modulated signal entering the receiver:

$$G a_1 = p_0 m e^{j\alpha}. \tag{6}$$

Since G relates an electrical amplitude to an optical power, it has the rather peculiar units of (optical power)/(square root of electrical power), i.e., the square root of power.

The electrical wave b_2 emanating from the receiver has two sources: the modulated optical power incident on the receiver and the electrical a_2 wave incident from the right-hand side and reflected back by the receiver's imperfect match.

We define the receiver's complex response R by

$$R \equiv \left.\frac{b_2}{m e^{j\alpha} p_0}\right|_{a_2 = 0}. \tag{7}$$

R describes the amplitude of the forward electrical wave created by an intensity modulated optical signal with modulation index m when $a_2 = 0$, i.e., when the receiver is connected to a matched load. Since R linearly relates an optical power to an

electrical amplitude, it has the units of one over the square root of power.

Since the electrical system is linear, we can add the signal generated by the optical wave incident on the receiver to the electrical wave it reflects from its electrical port to obtain $b_2 = \Gamma_r a_2 + Rp_0 m e^{j\alpha}$, where Γ_r is the electrical reflection coefficient of the receiver.

Combining (6) with the above relation, we obtain the following equations relating the electrical waves with frequency ω at ports 1 and 2:

$$\begin{aligned} b_1 &= \Gamma_m a_1 \\ b_2 &= \Gamma_r a_2 + RGa_1. \end{aligned} \tag{8}$$

These equations can be written in matrix form as

$$\begin{bmatrix} b_1 \\ b_2 \end{bmatrix} = \begin{bmatrix} \Gamma_m & 0 \\ RG & \Gamma_r \end{bmatrix} \begin{bmatrix} a_1 \\ a_2 \end{bmatrix} \equiv \begin{bmatrix} S_{11} & S_{12} \\ S_{21} & S_{22} \end{bmatrix} \begin{bmatrix} a_1 \\ a_2 \end{bmatrix} \tag{9}$$

giving the electrical scattering matrix for the total system comprised of the laser, modulator, and receiver.

IV. Measurement of R and G in a Coaxial System

Now that we have built a framework for our optoelectronic measurements, measurement of R or G with a calibrated electrical VNA is straightforward. First, we calibrate the VNA with a full two-port calibration with a 50-Ω reference impedance Z_r and use it to measure the scattering parameters of a modulated optical source connected to our calibrated reference receiver with known response R (see Fig. 2). Using (9), we determine the response G of the optical modulator from $G = S_{21}/R$ and its reflection coefficient Γ_m from S_{11}, completing characterization of the modulator. If we replace our calibrated reference receiver with an uncharacterized receiver, we can repeat the procedure and determine the uncharacterized receiver's response from $R' = S'_{21}/G$, and its reflection coefficient Γ'_r from S'_{22}, where the primed quantities refer to the measurements of the second receiver.

Our calibration approach uses a complex response R that accounts for both the magnitude and phase response of the reference receiver. In the past, calibration of the phase response of the reference receiver has relied on methods that are not traceable to fundamental physical principles. In [11], a VNA and a model of the modulator was used to estimate the phase response of the reference receiver. An oscilloscope whose response was derived from a model was used in [12] to estimate the phase response of a receiver. Also, oscilloscopes that were calibrated with the nose-to-nose method (described in [13] and [14]) were used to characterize the phase response of receivers in [15]. A recently developed method for measuring both the magnitude and phase response of an optical receiver, which can be made traceable to fundamental physical principles, is described in [16] and [17]. Traceable measurement of the response phase of a reference receiver is currently an area of intense research and is outside the scope of this tutorial.

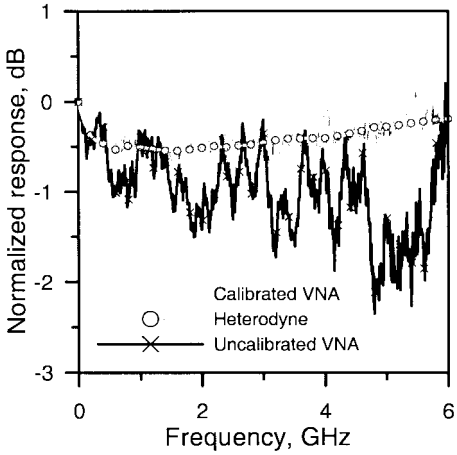

Fig. 3. Comparison of measured normalized response ($20\log(\Re)$), described in Appendix I) of a commercial optical receiver. The data has also been normalized to 0 dB at the lowest frequency. The expanded uncertainty (2σ) in the heterodyne measurements is approximately 0.12 dB.

V. Measurement Example

We applied the method described above to determine the magnitude response of a commercial receiver. We used an integrated Mach–Zehnder modulator in the experiment, and we calibrated the response magnitude of our reference receiver with the heterodyne method of [18] and microwave corrections of [1]. The heterodyne measurement method is used in standards laboratories because it is traceable to fundamental physical principles and can be implemented with a very low uncertainty [19].

Fig. 3 compares our normalized VNA measurement to a direct heterodyne measurement performed with the procedures of [18] and [1], which has a typical combined standard uncertainty of approximately 0.06 dB. The calibrated VNA curve is noisy because of the weak signal from the unamplified receiver, which is operating at a low photocurrent to maintain receiver linearity. Nevertheless, this figure demonstrates the accuracy of the procedure based on a calibrated VNA and calibrated reference receiver.

To illustrate the importance of the corrections performed by the network analyzer, we turned off the network analyzer's calibration and repeated the measurement. The uncalibrated VNA curve of Fig. 3 clearly shows the importance of corrections and the need for calibrating the network analyzer.

VI. Linearity

As mentioned above, the linearity of the receiver is an important consideration. The unmodulated portion p_0 of the optical signal flowing through the modulator can saturate the response of the receiver [20]. Reference receivers with a high compression point minimize this effect. Examples of highly linear receives are given in [21]–[23]. You can verify linear operation by changing p_0 to αp_0 (where $\alpha \approx 0.5$) and verifying that S_{21} changes to αS_{21}, within an acceptable level of accuracy.

VII. Scattering Matrices of Individual Optoelectronic Components

The electrical behavior of any modulator–receiver pair satisfying the basic assumptions we employed in this study can be analyzed with the scattering matrix (9). However, the scattering parameters of a modulator–receiver pair can be formally decomposed into a scattering matrix $\tilde{S}_m$ for the modulator and a scattering matrix $\tilde{S}_r$ for the receiver with

$$\tilde{S}_m \equiv \begin{bmatrix} \Gamma_m & 0 \\ G & 0 \end{bmatrix}$$
$$\tilde{S}_r \equiv \begin{bmatrix} 0 & 0 \\ R & \Gamma_r \end{bmatrix}. \tag{10}$$

These matrices have the properties that, when cascaded using the conventional rules for combining electrical circuits outlined in [5] and [6], they give the matrix (9). That is, when $\tilde{S}_m$ and $\tilde{S}_r$ are converted into cascade matrices (as described in Appendix IV), multiplied together, and the matrix product is reconverted to a scattering matrix, the result is the scattering matrix (9) of the modulator–receiver pair. This is true despite the fact that G and R have dimensions, whereas the elements of conventional scattering matrices are dimensionless. Since they differ from conventional scattering matrices, we denote the optoelectronic scattering matrices with a tilde and we do *not* call G and R scattering parameters.

Decomposing the scattering matrices of the system with (10) has no fundamental advantage over treating the modulator and receiver as a pair and using (9). However, this decomposition does make it possible to summarize the properties of a single optoelectronic component with a scattering matrix.

Furthermore, the description of the electrical waves at the electrical ports in this formalism is consistent with that of standard microwave circuit theory. As a result, we may cascade or deembed (remove) electrical circuits from the electrical port of optoelectronic components characterized in this way using the conventional rules outlined in Appendix IV and in [5] and [6].

For example, after measuring the scattering matrix $\tilde{S}_r$ of an optical receiver, we can cascade the electrical scattering parameters of an amplifier onto the electrical port of the receiver and determine the scattering parameters of the combination. This is done by converting $\tilde{S}_r$ and the scattering parameters of the amplifier into cascade matrices, multiplying these cascade matrices together, and reconverting the matrix product back into a scattering matrix. The procedure is also explained in Appendix IV and in detail in [5] and [6].

VIII. On-Wafer Measurement Example

If we determine the scattering matrix $\tilde{S}_m$ of a modulator using the method above, we can substitute the reference receiver with the on-wafer-receiver/wafer-probe combination shown in Fig. 4. This combined receiver has optical and coaxial ports that are compatible with those of the reference receiver.

To characterize the on-wafer optical receiver between the optical port and the CPW reference plane, we can now deembed (remove) the effect of the probe from the measurement of the combined response of the on-wafer receiver and probe. This can be accomplished by converting the scattering matrix $\tilde{S}_{rp}$ of the receiver and probe combination and the scattering matrix S_p of the probe alone, as determined by a two-tier calibration procedure [24], into cascade matrices $\tilde{T}_{rp}$ and T_p. We obtain the cascade matrix $\tilde{T}_r$ of the on-wafer receiver alone by multiplying $\tilde{T}_{rp}$ by the *inverse* cascade matrix for the probe head

$$\tilde{T}_r = \tilde{T}_r T_p T_p^{-1} = \tilde{T}_{rp} T_p^{-1}. \tag{11}$$

Finally, we reconvert the cascade matrix $\tilde{T}_r$ back into a scattering matrix. Reference [25] also gives a procedure for deembedding the scattering matrix of an optical receiver or laser from a probe head. However, the mathematical formalism described here is much more straightforward and compact.

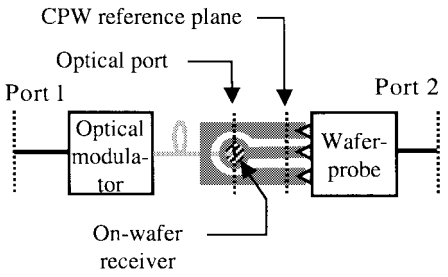

Fig. 4. Schematic of on-wafer receiver measurement showing coaxial reference planes at ports 1 and 2, the optical reference plane at the fiber output, and the coplanar waveguide (CPW) reference plane. The response of the on-wafer receiver is defined by the optical and CPW reference planes and the response of the wafer probe is defined by the CPW reference plane and the coaxial reference plane at port 2.

IX. Discussion of Restrictions

It is important to keep in mind the restrictions of this theory at the optical ports. At the optical ports, we required that, for a single-frequency electrical excitation, the intensity modulation of the optical carrier be of the form given in (4) and that there be no reverse optical wave. These requirements were needed to develop the relations in (6) and (9). Among other things, they eliminate the effects of coherent optical interference on the measurements observed in [11]. These effects are not accounted for by the theory and are left uncharacterized by the instrumentation.

A simple thought experiment illustrates the need to eliminate the backward-traveling optical power at the optical port. Imagine that you have assembled and calibrated a test set consisting of a VNA, optical modulator, and optical receiver, and that the optical modulator and receiver are engineered to not reflect any of the optical power incident upon them, as good engineering practice would dictate.

Now consider what happens when you test an imperfect optical modulator that reflects some percentage q_m of the backward optical wave incident upon it and that is connected to a short piece of nonreflective optical fiber. The total gain G of the optical modulator and fiber will be reduced somewhat from the gain of the optical modulator alone due to the reflection at its output, but will be otherwise unaffected.

If you test a short piece of optical fiber driving an imperfect optical receiver that reflects some percentage q_r of the forward

optical power incident upon it, the total response R you measure will also be reduced somewhat from the response of the optical receiver alone, but again, will be otherwise unaffected.

However, when you connect the optical-modulator/output-fiber/input-fiber/optical-receiver combination together, you create an optical resonator in the optical fiber between the modulator and receiver. The response of this optical resonator will depend sensitively on the optical frequency and chirp of the optical carrier from the modulator, the coherence length of the optical source, the exact distance in *optical* wavelengths between the modulator and receiver, and the loss in the optical fibers forming the resonator. Most importantly, the sharp wavelength dependence of the optical resonator would change not only the overall magnitude and phase of the microwave modulation on the optical carrier, but also its shape, adding additional (and unexpected) electrical harmonics into the system. That is, the filtering nature of the resonator could remove power from the fundamental of the drive frequency in a way that depends on the exact wavelength of the optical carrier, which is also not characterized by our measurement system. As a result, the separate measurements of the individual optoelectronic components would not predict the performance of the system.

Now let us examine two limiting cases of the optical coherence. If the optical source has a coherence length much greater than the distance between the modulator and receiver, submicrometer changes in the optical path length will cause the measured optical signal to vary by a significant amount. This variation is not described by our formalism, which only accounts for effects that change the modulation envelope, nor is it accounted for in commercially available LCAs. Even if the source has a very short coherence length, the positions of the reflections and their reflection coefficients must be measured for a complete characterization of the system. Again, this information is not available in the simple measurement system shown in Fig. 2 or in commercial LCAs.

Accounting for the optical reflections and coherence would greatly complicate the measurement of simple optoelectronic components, and we need not account for them if there are no back reflections in our system. Our restrictions are easily (and usually) satisfied in common microwave applications [26], [27] and in systems for measuring modulator, laser, and receiver response by using good design practices. These commonly used practices include using wedged dielectric interfaces, antireflective coatings, and optical isolators.

Our restrictions, however, and the lack of information on the optical carrier prevent us from developing scattering-parameter representations for many optical/optical components, as was done in [28] and [29], and for optical/electronic components, as was done in [30]. For example, it is not possible to develop a scattering-parameter representation for optical/optical or optical/electronic components if those components generate optical reflections, if they are dispersive, or if they filter the optical signal, for example, by eliminating the optical carrier or one of the sidebands. Any formalism capable of accounting for these effects would require information about the wavelength, phase, and coherence length of the optical carrier [31]; information not contained in the scattering-parameter formalism described here or in [28]–[30]. Although these properties could, in principle, be characterized with supplemental measurements and instrumentation, the formalism would also have to be capable of accounting for the *additional* electrical harmonics introduced into the system by optical/optical components that filter the optical sidebands of the modulated optical signal.

X. Conclusions

We have described a straightforward procedure for characterizing optical modulators and receivers with a calibrated VNA and a calibrated reference receiver. The method only requires that the modulated optical source linearly modulate the optical power, that the receiver respond linearly to this modulated optical power, that the optical power at the optical port have the form of (4), and that there be no reflected optical power at the optical port connecting the modulator and receiver. Within the constraints of these assumptions, the formalism is rigorous and consistent with common practice for electrical network measurements.

Appendix I
Relating R and Normalized Frequency Response $\Re^2$

Sometimes normalizing the output of the signal of the receiver (photodiode) to the generated photocurrent is better than normalizing to the input optical power, i.e., the normalized frequency response $\Re^2$ may be a better characterization of the receiver than R. This might be the case when the dc responsivity η of a fiber-connectorized receiver is poorly characterized because the connector insertion loss is not repeatable [32], [33] or when η is unknown. The heterodyne method [18] is commonly used to measure $\Re^2$.

The normalized frequency response $\Re^2$ is defined as

$$\Re^2 \equiv \frac{P_{\rm rf}}{\frac{1}{2}\, i_{\rm dc}^2 m^2 Z_r} \tag{12}$$

where $P_{\rm rf}$ is the RF power the receiver delivers to a 50-Ω load and $i_{\rm dc}$ is the dc photocurrent drawn by the receiver when illuminated by the constant component p_0 of the optical signal. The relations $P_{\rm rf} = \frac{1}{2}|b_2|^2$ and $i_{\rm dc} = \eta p_0$ give

$$\Re^2 = \frac{\frac{1}{2}|b_2|^2}{\frac{1}{2}\,(p_0\eta)^2 m^2 Z_r} \tag{13}$$

where η is the dc responsivity of the receiver, in amperes per watts, when driving a 50-Ω load. Applying (7) gives the relation between R and $\Re^2$ as follows:

$$\Re^2 = \frac{|R|^2}{\eta^2 Z_r}. \tag{14}$$

Appendix II
Measuring the Normalized Frequency Response $\Re^2$

The normalized frequency response can be directly measured with a calibrated VNA system when p_0 and m can be varied

independently, such as when the optical source (laser) is externally modulated. The normalized frequency response $\Re'^2$ of an unknown receiver is determined from

$$\Re'^2 = \left|\frac{S'_{21}(p'_0)}{S_{21}(p_0)}\right|^2 \Re^2, \qquad \text{when } i'_{\rm dc} = i_{\rm dc} \tag{15}$$

where $\Re^2$ is the normalized frequency response of the reference receiver used to calibrate the system. Here, the average optical power p'_0 must be adjusted until $i'_{\rm dc}$, the photocurrent from the unknown receiver, is matched to $i_{\rm dc}$, the photocurrent from the reference receiver, by varying the optical source power. Here, S_{21} and S'_{21} (the forward transmission coefficients for the measurement system with the reference and unknown receivers, respectively) are functions of the optical power at which they are measured.

We derived (15) using the definition of S_{21} in (9) and expand G using (6). While p_0 changes, a_1 and m are kept constant. After canceling like terms, we obtain the ratio

$$R' = \frac{S'_{21}(p'_0)}{S_{21}(p_0)} \cdot \frac{p'_0 R}{p_0} = \frac{S'_{21}(p'_0)}{S_{21}(p_0)} \cdot \frac{\eta R}{\eta'}. \tag{16}$$

The last step in (16) was made using the constraint $p_0\eta = p'_0\eta'$. Since η and η' may not be equal, we need to vary p_0 to maintain this constraint. Squaring and using (14) gives (15), which is the desired result.

Appendix III
Relation Between Measurements and Equivalent-Circuit Models

Here, we relate our measured receiver response R to standard Thévenin and Norton equivalent-source models, and we relate the modulator response G to the input drive voltage and current.

The Thévenin equivalent voltage v_T of the receiver with input given by (4) is equal to the voltage that the receiver generates across an open circuit. To solve for v_T, we use the fact that the amplitude of the wave reflected by the open circuit is equal to the amplitude of the wave incident upon it. Thus, we can set $a_2 = b_2$ in the second equation in (8), which gives

$$b_2 = Rp_0 m e^{j\alpha}(1-\Gamma_r)^{-1}. \tag{17}$$

We can rewrite (1) as

$$\begin{aligned} v &= \sqrt{Z_r}(a+b) \\ i &= \frac{1}{\sqrt{Z_r}}(a-b) \end{aligned} \tag{18}$$

which we combine with (17) to obtain

$$v_T \equiv v_2\big|_{\rm open} = 2\sqrt{Z_r}\, b_2 = (p_0 m e^{j\alpha})\,\frac{2\sqrt{Z_r}R}{(1-\Gamma_r)}. \tag{19}$$

The Norton equivalent current i_N of the receiver is the outgoing current the receiver generates across a short circuit. In this case, $a_2 = -b_2$. Using (8) and (18), we obtain

$$i_N \equiv -i_2\big|_{\rm short} = (mp_0 e^{j\alpha})\,\frac{2R}{\sqrt{Z_r}(1+\Gamma_r)}. \tag{20}$$

The responsivity of the receiver (in volts per watt or amperes per watt) can be obtained by dividing the source voltage or current by $mp_0 e^{j\alpha}$.

The small-signal current response (ac current slope efficiency) η_i of a modulator or laser is the ratio of the optical power modulation to the input drive current. We will now find η_i in terms of the measured quantities G and Γ_m. We use (18) to find the current and voltage at the input port in terms of a_1 and the modulator's reflection coefficient $\Gamma_m = b_1/a_1$

$$\begin{aligned} v_1 &= \sqrt{Z_r}\, a_1(1+\Gamma_m) \\ i_1 &= \frac{a_1}{\sqrt{Z_r}}(1-\Gamma_m). \end{aligned} \tag{21}$$

The current modulation response η_i is found by substituting a_1 from (6) into (21), and solving for the optical modulation per ampere drive, which gives

$$\eta_i \equiv \frac{mp_0 e^{j\alpha}}{i_1} = \frac{G\sqrt{Z_r}}{1-\Gamma_m}. \tag{22}$$

The small-signal voltage response (ac voltage slope efficiency) η_v of a modulator or laser is the ratio of the optical power modulation to the input drive voltage. The voltage modulation response η_v is found by substituting a_1 from (6) into (21) and solving for the optical modulation for a given input drive voltage, from which we obtain

$$\eta_v \equiv \frac{mp_0 e^{j\alpha}}{v_1} = \frac{G}{\sqrt{Z_r}\,(1+\Gamma_m)}. \tag{23}$$

The π-voltage V_π is a commonly specified property of an electrooptic modulator, defined in terms of the large-signal model (transfer function) of the modulator [34]

$$p(t) = p_0\left[1+\sin\left(\frac{\pi {\rm Re}(v_1 e^{j\omega t})}{V_\pi}\right)\right]. \tag{24}$$

That is, V_π is the input voltage that gives a change of π in the argument of the modulator's transfer function. When $|v_1| \ll V_\pi$, we can approximate (24) by the first term of its Taylor series expansion to give the small-signal modulation

$$p(t) \simeq p_0 + \frac{\pi p_0 |v_1|}{V_\pi}\cos(\omega t + \arg(v_1) + \beta) \tag{25}$$

where β accounts for a delay between the input drive voltage and output optical modulation. Hence, the small-signal modulation depth $m = \pi|v_1|/V_\pi$ can be found by equating (25) with (4). Substituting into (23) gives V_π in terms of G and Γ_m

$$V_\pi = \frac{\pi p_0}{|G|}\sqrt{Z_r}\,|1+\Gamma_m|. \tag{26}$$

Appendix IV
Cascade Matrices

Fig. 5 shows two components connected together in series. We wish to find the scattering matrix $S_{\rm Total}$ that describes the series combination using the scattering matrices S_A and S_B that characterize the individual components. Since the scattering matrix does not relate the a and b waves at an input port to the a

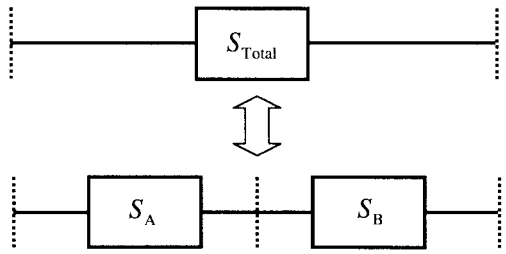

Fig. 5. Components, individually described by scattering matrices S_A and S_B, when connected in series can be described by a combined scattering matrix S_{Total}.

and b waves at an output port, we cannot multiply the individual scattering matrices of the adjacent components in Fig. 5 to obtain the total scattering matrix, i.e.,

$$S_{\text{Total}} \neq S_A S_B. \tag{27}$$

The cascade matrix $[T]$ [5] defined by

$$\begin{bmatrix} b_1 \\ a_1 \end{bmatrix} = \begin{bmatrix} T_{11} & T_{12} \\ T_{21} & T_{22} \end{bmatrix} \begin{bmatrix} a_2 \\ b_2 \end{bmatrix} \tag{28}$$

relates waves at one port to the waves at another port. The cascade matrix (28) is also sometimes referred to as a transmission matrix or a T-matrix. The total cascade matrix T_{Total} of the components in series is

$$T_{\text{Total}} = T_A T_B. \tag{29}$$

The elements of the cascade matrix can be found in terms of the scattering matrix elements by relating (3) and (28) to obtain

$$[T] = \frac{1}{S_{21}} \begin{bmatrix} S_{12}S_{21} - S_{11}S_{22} & S_{11} \\ -S_{22} & 1 \end{bmatrix} \tag{30}$$

and the cascade matrix is converted back to a scattering matrix using the transformation

$$[S] = \frac{1}{T_{22}} \begin{bmatrix} T_{12} & T_{11}T_{22} - T_{12}T_{21} \\ 1 & -T_{21} \end{bmatrix}. \tag{31}$$

Appendix V
Calibration of an LCA

In this section, we discuss a method for calibrating an LCA that has the architecture shown in Fig. 6. The LCA has two electrical ports $\mathcal{E}_1$ and $\mathcal{E}_2$, as well as an optical output port $\mathcal{O}_1$ and optical input port $\mathcal{O}_2$. By setting the switches appropriately, this analyzer can be used to characterize components with two electrical ports, or with one electrical and one optical port. In the following discussion, we show how this analyzer can be calibrated with methods similar to those we described in Section IV.

As before, calibration begins with a full 50-Ω two-port electrical scattering-parameter calibration at the electrical ports $\mathcal{E}_1$ and $\mathcal{E}_2$ performed with the switches in Fig. 6(a) both in the "up" position. This calibration corrects for imperfections in the VNA, as well as the switches and cables between the analyzer and

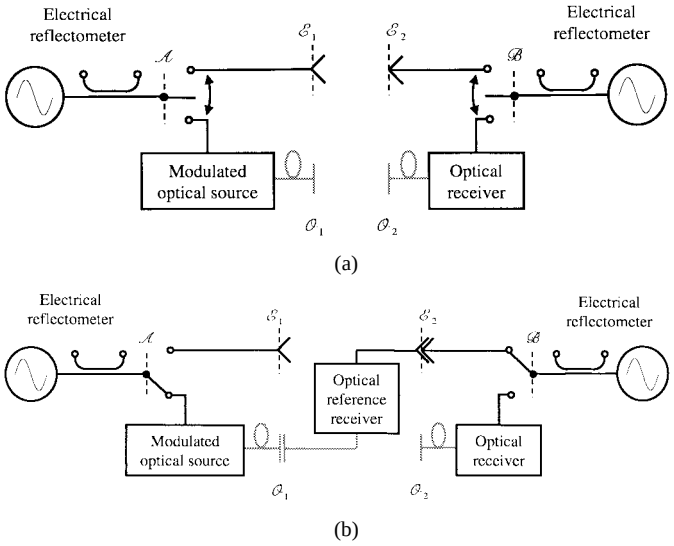

Fig. 6. (a) Simplified schematic of an LCA. (b) How a calibrated reference receiver is connected to the LCA during calibration.

reference planes $\mathcal{E}_1$ and $\mathcal{E}_2$. Using this calibration, a measurement of the reference receiver [as sketched in Fig. 6(b)] determines the scattering parameters corresponding to the product $T_A^{-1}\tilde{T}_m\tilde{T}_r$, where T_A is the cascade matrix of the switch and cable between $\mathcal{A}$ and $\mathcal{E}_1$, $\tilde{T}_m$ is the cascade matrix of the modulator between reference plane $\mathcal{A}$ and reference plane $\mathcal{O}_1$, and $\tilde{T}_r$ is the cascade matrix of the calibrated reference receiver. Thus, when we extract G and Γ_m from (9), instead of determining the gain and reflection coefficient of the modulator, we determine instead the response G and reflection coefficient Γ_m of the circuit corresponding to $T_A^{-1}\tilde{T}_m$.

However, if we now connect an uncharacterized optical receiver between $\mathcal{O}_1$ and $\mathcal{E}_2$, we measure the scattering parameters corresponding to the circuit $T_A^{-1}\tilde{T}_m\tilde{T}_r'$, where $\tilde{T}_r'$ is the transmission matrix of the as-yet uncharacterized receiver. Thus, we can still determine the uncharacterized receiver's response R' from $R' = S_{21}'/G$ and its reflection coefficient Γ_r' from S_{22}, as G refers to the gain of the circuit corresponding to $T_A^{-1}\tilde{T}_m$ that we wish to remove from the measurement $T_A^{-1}\tilde{T}_m\tilde{T}_r'$.

Calibrating the receiver arm of the LCA proceeds in a similar fashion. With port $\mathcal{O}_1$ connected directly to $\mathcal{O}_2$ and both of the switches in the "down" position, we measure the scattering parameters corresponding to the product $T_A^{-1}\tilde{T}_m\tilde{T}_r''T_B^{-1}$, where T_B is the cascade matrix of the path from reference plane $\mathcal{E}_2$ to reference plane $\mathcal{B}$ and $\tilde{T}_r''$ is the cascade matrix of the analyzer's receiver situated between $\mathcal{O}_2$ and $\mathcal{B}$. Thus, when we use the gain G corresponding to the circuit $T_A^{-1}\tilde{T}_m$ characterized earlier, we determine the response and reflection coefficient of the circuit corresponding to $\tilde{T}_r''T_B^{-1}$. This is exactly what we need to calibrate measurements of optical modulators connected between $\mathcal{E}_1$ and $\mathcal{O}_2$ and tested with switch $\mathcal{A}$ in the "up" position and switch $\mathcal{B}$ in the "down" position.

References

[1] P. D. Hale, T. S. Clement, and D. F. Williams, "Know your response: Measuring frequency response of high-speed optical receivers requires microwave measurements," *SPIE Mag.*, p. 55, Mar. 2001.

[2] "High-speed lightwave component analysis," Agilent Technologies, Palo Alto, CA, Applicat. Note 1550-6, June 2000.

[3] T. S. Clement, P. D. Hale, and P. A. Williams, "Fiber and component metrology for high-speed communications: What the manual doesn't tell you," in *Optical Fiber Communications Conf. Dig.*, Mar. 2002, Tutorial Sessions, Session W-Z.
[4] P. D. Hale, D. F. Williams, and T. S. Clement, "Calibrated high-speed optoelectronic measurements," presented at the IEEE MTT-S Int. Microwave Symp. Dig. Workshop Notes, June 2002, Workshop WMC.
[5] D. M. Kerns and R. W. Beatty, Eds., *Basic Theory of Waveguide Junctions and Introductory Microwave Network Analysis*. New York: Pergamon, 1967.
[6] R. B. Marks and D. F. Williams, "A general waveguide theory," *J. Res. Nat. Inst. Stand. Technol.*, vol. 97, pp. 533–562, 1992.
[7] V. Ramaswamy, M. D. Divino, and R. D. Standley, "Balanced bridge modulator switch using Ti-diffused $LiNbO_3$ strip waveguides," *Appl. Phys. Lett.*, vol. 32, pp. 644–646, 1978.
[8] B. E. A. Saleh and M. C. Teich, Eds., *Fundamentals of Photonics*. New York: Wiley, 1991, pp. 702–703.
[9] R. L. Jungerman, C. Johnson, D. J. McQuate, K. Salomaa, M. P. Zurakowski, R. C. Bray, G. Conrad, D. Cropper, and P. Hernday, "High-speed optical modulator for application in instrumentation," *J. Lightwave Technol.*, vol. 8, pp. 1363–1370, Jan. 1990.
[10] B. H. Kolner and D. W. Dolfi, "Intermodulation distortion and compression in an integrated electrooptic modulator," *Appl. Opt.*, vol. 26, pp. 3676–3680, 1987.
[11] D. R. Harkins and M. A. Heinzelman, "Accuracy considerations and error correction techniques for 20 GHz lightwave component analysis," *Hewlett-Packard J.*, pp. 34–40, 1991.
[12] R. T. Hawkins, M. D. Jones, S. H. Pepper, J. H. Goll, and M. K. Ravel, "Vector characterization of photodetectors, photoreceivers, and optical pulse sources by time-domain pulse response measurements," *IEEE Trans. Instrum. Meas.*, vol. 41, pp. 467–475, Aug. 1992.
[13] J. Verspecht, "Broadband sampling oscilloscope characterization with the nose-to-nose calibration procedure: A theoretical and practical analysis," *IEEE Trans. Instrum. Meas.*, vol. 44, pp. 347–354, Dec. 1995.
[14] P. D. Hale, T. S. Clement, K. J. Coakley, C. M. Wang, D. C. DeGroot, and A. P. Verdoni, "Estimating magnitude and phase response of a 50 GHz sampling oscilloscope using the 'nose-to-nose' method," in *55th ARFTG Conf. Dig.*, June 2000, pp. 335–342.
[15] T. S. Clement and P. D. Hale, "Photoreceiver measurements using 50 GHz sampling oscilloscope with frequency domain corrections," in *Optical Fiber Measurements Tech. Dig. Symp.*, Sept. 2000, pp. 121–124.
[16] D. F. Williams, P. D. Hale, T. S. Clement, and J. M. Morgan, "Calibrating electro-optic sampling systems," in *IEEE MTT-S Int. Microwave Symp. Dig.*, May 2001, pp. 1527–1530.
[17] T. S. Clement, D. F. Williams, P. D. Hale, and J. M. Morgan, "Calibrated photoreceiver response to 110 GHz," in *IEEE LEOS Annu. Meeting Dig.*, Nov. 2002, pp. 877–878.
[18] P. D. Hale, C. M. Wang, R. Park, and W. Y. Lau, "A transfer standard for measuring photoreceiver frequency response," *J. Lightwave Technol.*, vol. 41, pp. 2457–2466, Nov. 1996.
[19] A. D. Gifford, D. A. Humphreys, and P. D. Hale, "Comparison of photodiode frequency response measurements to 40 GHz between NPL and NIST," *Electron. Lett.*, vol. 31, pp. 397–398, 1995.
[20] P. L. Liu, K. I. J. Williams, M. Y. Frankel, and R. D. Esman, "Saturation characteristics of fast photodetectors," *IEEE Trans. Microwave Theory. Tech.*, vol. 47, pp. 1297–1303, July 1999.
[21] G. A. Davis, R. E. Weiss, R. A. LaRue, K. J. Williams, and R. D. Esman, "A 920–1650-nm high-current photodetector," *IEEE Photon. Technol. Lett.*, vol. 8, pp. 1373–1375, Oct. 1996.
[22] S. Demiguel, P. Pagnad-Rossiaux, E. Boucherez, C. Jany, L. Carpentier, V. Coupe, F. Devaux, L. Giraudet, S. Fock-Yee, and J. Decobert, "Design, optical, and high frequency characteristics of double stage tapered photodiodes for $>$40 Gb/s applications," in *IEEE LEOS Annu. Meeting Dig.*, Nov. 2001, Paper ThAA4, WC31-3.
[23] A. Stohr, R. Heinzelmann, A. Malcoci, and D. Jager, "Ultra-broadband 160 GHz InGaAsP photodetector for photonic LO," in *Proc. 27th Eur. Optical Communications Conf.*, 2001, Paper ThM.2.6, pp. 562–563.
[24] R. F. Bauer and P. Penfield, "De-embedding and unterminating," *IEEE Trans. Microwave Theory. Tech.*, vol. MTT-22, pp. 282–288, Mar. 1974.
[25] P. Debbie and L. Martens, "Measuring on-wafer high-frequency modulation response characteristics of optical transmitters and detectors," *IEEE Trans. Instrum. Meas.*, vol. 45, pp. 504–510, Apr. 1996.
[26] T. A. Cusick, S. Iezekiel, R. E. Miles, S. Sales, and J. Capmany, "Synthesis of all-optical microwave filters using Mach–Zehnder lattices," *IEEE Trans. Microwave Theory. Tech.*, vol. 45, pp. 1458–1462, Aug. 1997.
[27] M. Y. Frankel, P. J. Mathews, and R. D. Esman, "Fiber-optic true time steering of an ultrawide-band receive array," *IEEE Trans. Microwave Theory. Tech.*, vol. 45, pp. 1522–1526, Aug. 1997.
[28] D. D. Curtis and E. Ames, "Optical test set for microwave fiber-optic network analysis," *IEEE Trans. Microwave Theory. Tech.*, vol. 38, pp. 552–559, May 1990.
[29] S. Iezekiel, C. M. Snowden, and M. J. Howes, "Scattering parameter characterization of microwave optoelectronic devices and fiber-optic networks," *IEEE Microwave Guided Wave Lett.*, vol. 1, pp. 233–235, Sept. 1991.
[30] B. Stockbroeckx, P. Dellisse, and A. Vander Vorst, "S-matrix definition for microwave-optical transducers," *Microwave Opt. Technol. Lett.*, vol. 7, pp. 803–806, 1994.
[31] Y. Weissman, Ed., *Optical Network Theory*. Norwood, MA: Artech House, 1992.
[32] B. Wong and H. Kosiorska, "Factory measurement solutions to predictable field performance of single mode fiber optic connectors," in *Technical Digest–Symposium on Optical Fiber Measurements 1992*. ser. Special Pub. 839, G. W. Day and D. L. Franzen, Eds. Boulder, CO: NIST, 1992, pp. 23–28.
[33] R. L. Gallawa and X. Li, "Calibration of optical fiber power meters: The effect of connectors," *Appl. Opt.*, vol. 46, pp. 1170–1174, 1987.
[34] A. Yariv and P. Yeh, Eds., *Optical Waves in Crystals*. New York: Wiley, 1984, pp. 280–281.

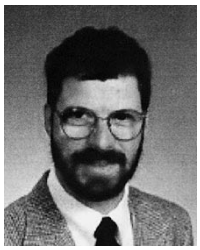

Paul D. Hale (M'01–SM'01) received the Ph.D. degree in applied physics from the Colorado School of Mines, Golden, CO, in 1989.

Since 1989, he has been a Staff Member with the National Institute of Standards and Technology (NIST), Boulder, CO, where he has conducted research in birefringent devices, mode-locked fiber lasers, fiber chromatic dispersion, broad-band lasers, interferometry, polarization standards, and high-speed optoelectronic measurements. He is currently Leader of the High-Speed Measurements Project in the Sources and Detectors Group, NIST. His research interests include high-speed optoelectronic and microwave measurements and their calibration.

Dr. Hale is currently an associate editor of the JOURNAL OF LIGHTWAVE TECHNOLOGY. He, along with a team of four scientists, was the recipient of the 1994 Department of Commerce Gold Medal for measuring fiber-cladding diameter with an uncertainty of 30 nm. He, along with four other scientists, was also the recipient of the 1998 Department of Commerce Bronze Medal for developing measurement techniques and standards to determine optical polarization parameters.

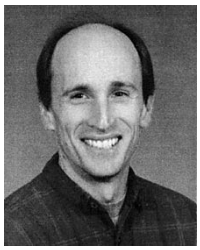

Dylan F. Williams (M'80–SM'90–F'02) received the Ph.D. degree in electrical engineering from the University of California at Berkeley, in 1986.

In 1989, he joined the Electromagnetic Fields Division, National Institute of Standards and Technology (NIST), Boulder, CO, where he develops metrology for the characterization of monolithic microwave integrated circuits and electronic interconnects. He has authored or coauthored over 80 technical papers.

Dr. Williams was the recipient of the Department of Commerce Bronze and Silver Medals, the Electrical Engineering Laboratory's Outstanding Paper Award, two ARFTG Best Paper Awards, the ARFTG Automated Measurements Technology Award, and the IEEE Morris E. Leeds Award.